

RESEARCH

Open Access



Single-cell RNA sequencing reveals the intra-tumoral heterogeneity and immune microenvironment of small cell carcinoma of the ovary, hypercalcemic type

Yi Gao^{1†}, Kewei Zheng^{1†}, Haowen Tan⁵, Mingyi Kang¹, Bingjian Lu⁴, Ling Chen⁶, Jing Xu¹, Chong Lu¹, Ranran Chai¹, Congjian Xu^{1,2,3*} and Yu Kang^{1*}

Abstract

Purpose Small cell carcinoma of the ovary, hypercalcemic type (SCCOHT) is a rare and lethal cancer lacking effective treatment. Its genomic mutations and tumor microenvironment need further exploration.

Methods We performed whole-exome sequencing or gene panel test to explore the SMARCA4 mutation spectrum in SCCOHT (15 samples). Single-cell RNA sequencing was conducted on one primary lesion with matched normal ovarian tissue and one recurrent lesion to investigate the intra-tumoral heterogeneity and immune microenvironment. Multiplex immunofluorescence staining validated T cell infiltration and PD-1 expression.

Results 13/15 (86.7%) patients harbored SMARCA4 mutations. The loss of heterozygosity (LOH) occurred in 10/15 (66.7%) patients. Cancer cells and immune cells were observed in SCCOHT tumors. Cancer cells were further divided into seven subtypes and one from recurrent lesion exhibited the highest stemness accompanied by high expression of genes related to cell mitosis (*AURKB*, *CHEK2*, *CCNB1*, *WEE1*), DNA repair (*BRCA1*, *RAD51*) and epigenetic (*EZH2*, *DNMT1*). Immune cells mainly included macrophages and T cells. Lipid-associated tumor-associated macrophages (TAMs) was mainly in primary lesion while inflammatory cytokine-enriched TAMs in recurrent lesion. $CD4^+ / CD8^+$ T cell infiltration was observed in SCCOHT tumor and a certain proportion of T cells expressed PD-1.

Conclusions SCCOHT exhibits universal SMARCA4 LOH and significant intra-tumoral heterogeneity, suggesting potential therapeutic targets, including CHEK2, CCNB1, and WEE1. Exhausted T cells and distinct TAM subsets infiltrate tumors. Targeting macrophage polarization or cytokine signaling may also be promising. These findings provide insights for developing novel therapies to improve outcomes in SCCOHT.

Clinical trial number Not applicable.

[†]Yi Gao and Kewei Zheng contributed equally to this work.

*Correspondence:
Congjian Xu
xucongjian@fudan.edu.cn
Yu Kang
yukang@fudan.edu.cn

Full list of author information is available at the end of the article



© The Author(s) 2025. **Open Access** This article is licensed under a Creative Commons Attribution-NonCommercial-NoDerivatives 4.0 International License, which permits any non-commercial use, sharing, distribution and reproduction in any medium or format, as long as you give appropriate credit to the original author(s) and the source, provide a link to the Creative Commons licence, and indicate if you modified the licensed material. You do not have permission under this licence to share adapted material derived from this article or parts of it. The images or other third party material in this article are included in the article's Creative Commons licence, unless indicated otherwise in a credit line to the material. If material is not included in the article's Creative Commons licence and your intended use is not permitted by statutory regulation or exceeds the permitted use, you will need to obtain permission directly from the copyright holder. To view a copy of this licence, visit <http://creativecommons.org/licenses/by-nc-nd/4.0/>.

Keywords SMARCA4, SCCOHT, Intra-tumoral heterogeneity, Immune microenvironment

Introduction

Small cell carcinoma of the ovary, hypercalcemic type (SCCOHT) is a rare and lethal cancer that mainly occurs in adolescents and young women [1]. Inactivating somatic and/or germline mutations in *SMARCA4*, a gene encoding a core subunit of the SWI/SNF chromatin remodeling complex, have been identified as the primary driver events in SCCOHT, with over 90% of cases harboring *SMARCA4* mutations [2–4].

Recent studies have also uncovered transcriptomic alterations in SCCOHT [5], prompting the development of targeted therapies, including epigenetic modulators, kinase inhibitors, and immunotherapies [6–8]. While these therapies have shown efficacy in some patients, responses remain inconsistent. Interestingly, despite the generally low tumor mutational burden (TMB) in SCCOHT, a subset of patients has benefited from immune checkpoint blockade, with studies revealing PD-L1 expression and significant T-cell infiltration in the majority of tumors [9]. These observations highlight the complexity of SCCOHT and underscore the need to better understand its tumor microenvironment, which remains poorly characterized.

In this study, we employed WES to analyze the genomic landscape of Chinese SCCOHT patients and single-cell RNA sequencing to comprehensively characterize transcriptomic changes, aiming to delineate the intra-tumoral heterogeneity and immune microenvironment of SCCOHT. Our findings provide novel molecular insights that may inform the development of more effective therapeutic strategies for this devastating disease.

Materials and methods

Patients and samples

A total of fifteen patients diagnosed with SCCOHT were recruited in this study, all of who were from the Obstetrics and Gynecology Hospital, Fudan University between 2015 and 2023. In this study, we aimed to include all available SCCOHT patients in our cohort without imposing specific inclusion or exclusion criteria to ensure a comprehensive and unbiased analysis. However, due to practical limitations such as time constraints, resource availability (e.g., manpower), and variations in patient access to healthcare, we were unable to collect all types of samples (e.g., frozen tissue, FFPE, or single-cell sequencing samples) from every patient, resulting in an uneven distribution of sample types across the cohort. We collected five frozen tissue samples and ten formalin-fixed, paraffin-embedded (FFPE) samples for whole-exome sequencing (WES) or gene panel test. We found

thirteen patients carrying the *SMARCA4* variants and conducted Sanger validation. We also performed single-cell RNA sequencing on three samples, including one primary lesion (SCC-09) matched with a normal ovarian tissue (SCC-09_N) from one patient, and one recurrent lesion (SCC-01) from intestinal metastases of another patient (Supplementary Fig. S1). All specimens used for single-cell RNA sequencing were obtained through open surgery.

DNA extraction and whole exome sequencing (WES)

The DNA from frozen tissues and blood samples was extracted using the QIAamp DNA Micro Kit (Qiagen), and the DNA from FFPE samples was extracted using Maxwell 16 FFPE Plus LEV DNA Purification Kit (Promega); all operations were performed following the manufacturer's instructions. 200ng genomic DNA of each sample was sheared to 150~200 bp fragments with Biorupter (Diagenode, Belgium). Paired-end sequencing was performed using the NovaSeq 6000 S4 Reagent Kit v1.5 (300 cycles) on Illumina NovaSeq 6000 platform (Illumina, San Diego, USA) by Sequanta Technologies (Shanghai, China).

Detection of LOH

Whole-exome sequencing (WES) was performed on the tumor specimens to determine the mutation frequency of *SMARCA4*. Given that *SMARCA4* is a tumor suppressor gene and its pathogenic mechanism involves loss of function, LOH will be present when the variant allele frequency (VAF) exceeds 50% (e.g., when the VAF of all SNPs around the pathogenic variant is over 60% or below 40%).

Single-cell dissociation

Tissues were stored in the sCelLiveTM Tissue Preservation Solution (Singleron) on ice after the surgery within 30 min. Specimens were washed with Hanks Balanced Salt Solution (HBSS) three times, minced into small pieces, and then digested with 3 mL sCelLiveTM Tissue Dissociation Solution (Singleron) by Singleron PythoN™ Tissue Dissociation System at 37 °C for 15 min. The cell suspension was collected and filtered through a 40-micron sterile strainer. Afterward, the GEXSCOPE® red blood cell lysis buffer (RCLB, Singleron) was added, and the mixture [Cell: RCLB = 1:2 (volume ratio)] was incubated at room temperature for 5–8 min to remove red blood cells. The mixture was then centrifuged at 300 × g 4 °C for 5 min to remove supernatant and suspended softly with PBS.

Single-cell RNA sequencing (scRNA-seq)

Single-cell suspensions (2×10^5 cells/mL) with PBS (HyClone) were loaded onto microwell chips using the Singleron Matrix® Single Cell Processing System. Barcoding Beads are subsequently collected from the microwell chip, followed by reverse transcription of the mRNA captured by the Barcoding Beads and to obtain cDNA, and PCR amplification. The amplified cDNA is then fragmented and ligated with sequencing adapters. The scRNA-seq libraries were constructed according to the protocol of the GEXSCOPE® Single Cell RNA Library Kits (Singleron) [10]. Individual libraries were diluted to 4 nM, pooled, and sequenced on Illumina NovaSeq 6000 with 150 bp paired-end reads.

Cell type annotation

Cell-ID is a multivariate approach that extracts gene signatures for each cell and performs cell identity recognition using hypergeometric tests (HGT) [11]. The cell type identity of each cluster was determined with the expression of canonical markers found in the DEGs using SynEcoSys database (Supplementary Table S2). Heatmaps/dot plots/violin plots displaying the expression of markers used to identify each cell type were generated by Seurat v3.1.2 DoHeatmap/DotPlot/Vln-plot. Except for cancer cells, the subtyping of non-malignant cell types applied harmony v1.0 to remove batch effect [12].

Differentially expressed genes (DEGs) analysis

To identify differentially expressed genes (DEGs), we used the scanpy.tl.rank_genes_groups() function based on Wilcoxon rank sum test with default parameters and selected the genes expressed in more than 10% of the cells in either of the compared groups of cells and with an average log(Fold Change) value greater than 1 as DEGs. Adjusted p value was calculated by benjamini-hochberg correction and the value 0.05 was used as the criterion to evaluate the statistical significance.

Pathway enrichment analysis

To investigate the potential functions of cancer cells, Gene Ontology (GO) and Kyoto Encyclopedia of Genes and Genomes (KEGG) analysis were used with the “clusterProfiler” R package v 3.16.1 [13]. Pathways with p_adj value less than 0.05 were considered significantly enriched. For Gene Set Variation Analysis (GSVA) pathway enrichment analysis, the average gene expression of each cell type was used as input data [14]. Gene Ontology gene sets including molecular function (MF), biological process (BP), and cellular component (CC) categories were used as reference.

Cell differentiation potential evaluation: CytoTRACE

CytoTRACE v0.3.3 [15] (a computational method that predicts the differentiation state of cells from single-cell RNA-sequencing data using gene counts and expression) was used to predict the differentiation potential of cell subpopulations.

Pseudotime trajectory analysis: monocle2

Cell differentiation trajectory of monocyte subtypes was reconstructed with the Monocle2 v 2.10.0 [16]. For constructing the trajectory, the top 2000 highly variable genes were selected by Seurat (v3.1.2) FindVairableFeatures(), and dimension-reduction was performed by DDRTree(). The trajectory was visualized by plot_cell_trajectory() function in Monocle2.

scRNA-seq based CNA detection

The InferCNV package [17] was used to detect the CNAs in SCCOHT malignant cells. T cells were used as baselines to estimate the CNAs of malignant cells. Genes expressed in more than 20 cells were sorted based on their loci on each chromosome. The relative expression values were centered to 1, using 1.5 standard deviation from the residual-normalized expression values as the ceiling. A slide window size of 101 genes was used to smoothen the relative expression on each chromosome, to remove the effect of gene-specific expression.

Cell-cell interaction analysis (CellPhoneDB)

The cell-cell interaction analysis was performed by CellPhoneDB v2.1.0 [18] based on known receptor–ligand interactions between two cell types/subtypes. Cluster labels of all cells were randomly permuted for 1000 times to calculate the null distribution of average ligand-receptor expression levels of the interacting clusters. Individual ligand or receptor expression was thresholded with a cutoff value based on the average log gene expression distribution for all genes across all the cell types. The significant cell-cell interactions were defined as p value < 0.05 and average log expression > 0.1, which were visualized with the circlize v0.4.10 R package.

Multiplex Immunofluorescence (mIF) staining

We performed mIF staining by the test kit (Cat#abs50015, absin) according to the manufacturer's protocol. The immunofluorescence markers used consisted of CD4(Cat#ab183685, Abcam), CD8 (Cat#D263403, Sangon Biotech), PD1(Cat#ab237728, Abcam), FOXP3(Cat#D260367, Sangon Biotech), DAPI (Cat#D9542, Sigma). The slides were scanned by a Vectra 3 automated high-throughput multiplexed biomarker imaging system (Perkin Elmer, Waltham, MA, USA) and analyzed using the inform image analysis software (Perkin Elmer, Waltham, MA, USA).

Hematoxylin-eosin staining (HE staining)

The paraffin sections were firstly conducted dewaxing and hydration and then put sections into Hematoxylin solution, rinsed with tap water. Then treated the section with Hematoxylin Differentiation solution, rinsed with tap water. Treated the section with Hematoxylin Bluing solution, rinse with tap water. Then placed the sections in sequence in 85% ethanol – 95% ethanol - Eosin dye. At last, dehydrated and sealed the slices and observed them under a microscope.

Immunohistochemistry (IHC)

First, paraffin sections were dewaxed to water. Antigen repair was performed using citrate buffer (pH6.0) with a steamer followed by endogenous peroxidase blocking and serum closure. Then the slide were incubated with primary antibody (anti-BRG1, Servicebio, Cat#GB11258, 1:400 dilution) overnight at 4°C. Goat anti-rabbit horseradish peroxidase-conjugated secondary antibody was used. The chromogenic reaction was performed with DAB.

Statistical analysis

We used GraphPad Prism 9.0 software to analyze and visualize the data. Comparisons were assessed using Student t test or one-way ANOVA. Statistical significance was defined as $P < 0.05$.

Results

Patient cohort

The cohort comprised fifteen patients with an average diagnosis of 25.6 years old (range, 10–38). Four patients had hypercalcemia. Three patients were diagnosed with stage I tumors; three with stage II; four with stage III;

three with stage IV and three were unknown. thirteen patients had tumors with a maximum diameter exceeding 10 cm. Five patients underwent chemotherapy before collecting specimens of recurrent lesions. All clinical information has been summarized in the Supplementary Table S1.

The histological review was performed by three experienced pathologists and the diagnosis of SCCOHT was confirmed by hematoxylin and eosin (H&E) staining and immunohistochemistry (IHC) staining of typical SCCOHT markers (Supplementary Fig. S2).

SMARCA4 mutation spectrum in SCCOHT

To analyze the genetic etiology of SCCOHT, we performed next generation sequencing on a series of tumors from fifteen SCCOHT cases. WES or gene panel test were performed on DNA isolated from fresh frozen and FFPE tumor samples. *SMARCA4*, a gene recurrent mutated in SCCOHT, bore inactivation mutations in thirteen of fifteen tumors validated by Sanger sequencing (Table 1). The mutations occurred throughout various exons and included frameshift, nonsense, and splice-site mutations with the highest frequency of occurrence (8 in 15, 53.3%). Two samples (SCC-03 and SCC-10) harbored two pathogenic variants in *SMARCA4*, suggesting biallelic inactivation (Fig. 1). It is worth mentioning that a deletion of exons 1–6 of *SMARCB1* in the tumor tissue was found instead of *SMARCA4* mutation in a pediatric case (SCC-06).

Given that SCCOHT has been reported to occur in families and about 60% mutations in *SMARCA4* are germline [19, 20], we also evaluated the mutation type in our cohort. Among these thirteen patients harboring *SMARCA4* mutations, eleven of them were matched

Table 1 *SMARCA4* mutation in sccohs

Sample ID	Germline mutation		Somatic mutation 1		Somatic mutation 2		<i>SMARCA4</i> IHC
	Gene	Protein	Gene	Protein	Gene	Protein	
SCC-01	c.3546+2T>C	Not applicable	LOH		Not applicable		Loss
SCC-02	Not present		c.2973+1G>A	Not applicable	LOH		Loss
SCC-03	Not present		c.939_940insT	p.A314fs	c.2631 C>A	p.Y877*	Loss
SCC-04	Not present		Not present		Not present		Normal
SCC-05	Not present		c.4170+1G>T	Not applicable	LOH		Loss
SCC-06	Not present		Not present		Not present		Normal
SCC-07	c.1742_1745del	p.K581fs	LOH		Not applicable		Loss
SCC-08	Not present		c.3081+1G>T	Not applicable	LOH		Loss
SCC-09	c.1119-2 A>G	Not applicable	LOH		Not applicable		Loss
SCC-10	Not available		c.2123+1G>T	Not applicable	c.2859+5G>A	Not applicable	Loss
SCC-11	Not available		c.2506-2 A>G	Not applicable	LOH		Loss
SCC-12	Not present		c.917_941del	p.Gln306fs	Not present		Loss
SCC-13	Not present		c.1709_1722del	p.Gln570ProfsTer76	LOH		Loss
SCC-14	c.274 C>T	p.Gln92Ter	LOH		Not applicable		Loss
SCC-15	c.3229 C>T	p.Arg1077Ter	LOH		Not applicable		Loss

Not applicable, germline and somatic mutations already identified; not available, DNA not available; not present, no mutation present; IHC, immunohistochemistry

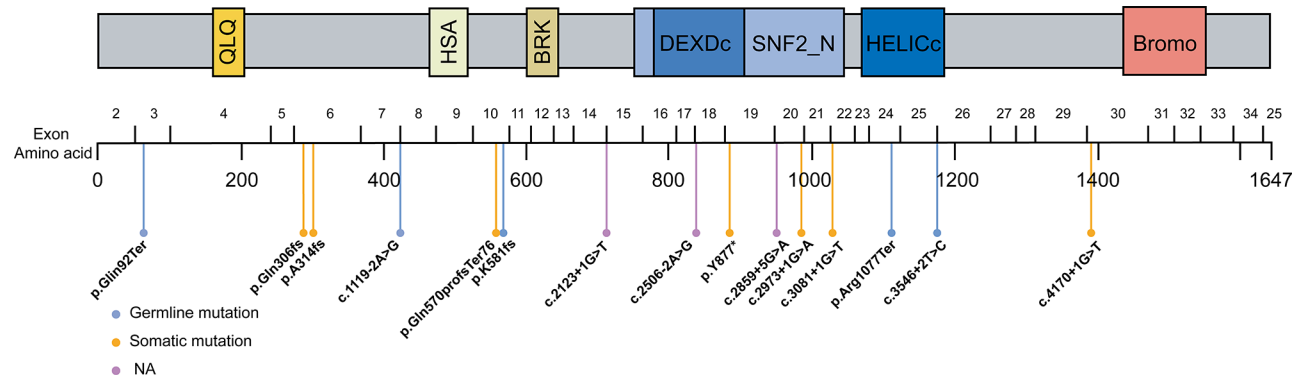


Fig. 1 Inactivating germline and somatic *SMARCA4* mutations identified in SCCOHT. A representation of the primary structure of the *SMARCA4* protein is shown with exon locations noted above. All germline mutations occurred in cohort are marked in blue, somatic mutations are in orange, and unknown types are marked by purple. QLQ, Gln, Leu, Gln motif; HSA, helicase/SANT-associated domain; BRK, Brahma and Kismet domain; DEXDc, DEAD-like helicase superfamily domain; SNF2_N, SNF2 family N-terminal domain; HELICc, helicase superfamily C-terminal domain; Bromo, bromodomain

with blood samples or normal tissues which gave us the chance to verify germline mutations. The results showed that the proportion of germline mutations in *SMARCA4* was 5/11 (45.5%), lower than previously reported data in literature. To evaluate the possible functional effects of mutations on the *SMARCA4* gene product, we assessed *SMARCA4* protein expression in SCCOHT tumors. All patients with *SMARCA4* mutations are accompanied by a loss of protein expression.

The loss of heterozygosity (LOH) of tumor suppressor genes leading to gene inactivation is believed to be related to the occurrence and development of tumors by somatic second hit [21]. We checked the allele fraction of *SMARCA4* mutation sites and found LOH in 10/15 (66.7%) cases (Table 1), suggesting that the LOH of *SMARCA4* may be one of the pathogenic mechanisms of SCCOHT.

Single-cell profiling of nonmalignant ovarian, primary, and recurrent SCCOHT tumor ecosystems

To systematically interrogate the intra-tumoral heterogeneity of SCCOHT, we performed scRNA-seq on one primary lesion (SCC-09_T) with matched normal ovarian tissue (SCC-09_N) from one patient and one recurrent lesion (SCC-01_T) from a different patient. A total of 29,808 cells were acquired from these samples following standard procedures. Of these, 20,174 cells (67.7%) were from SCCOHT tumors and 9634 (32.3%) were from nonmalignant ovary. These cells were then categorized into 8 clusters and annotated according to the established gene marker list by the canonical markers. Visualization of the cells was performed using UMAP approaches, as shown in Fig. 2A. Furthermore, Fig. 2B and C demonstrates the identification of cell types, including T-cell lineages (marked by *CD3D*, *CD2*, *TRBC2*), mononuclear phagocytes (*LYZ*, *CD14*, *C1QB* and *CD1C*), mural cells (*ACTA2*, *RGS5*, *PDGFRB* and *MYH11*), endothelial

cells (*CDH5*, *PECAM1*, *VWF* and *CLDN5*), cancer cells (*COL1A1*, *PCDH9*, *PTHLH*, *STMN1* and *SOX4*), granulosa cells (*AMH*, *HSD17B1*, *SERPINE2*, *NR5A2* and *GSTA1*), fibroblasts (*DCN*, *LUM*, *COL1A2*, *COL1A1*) and theca cells (*PTH1R*, *APOD*, *APOC1*, *WFDC1* and *COLEC11*). To verify the reliability of cell grouping, the InferCNV pipeline used T-cell lineages as the baseline to analyze copy number variations in the cancer cells. The cancer cells had obvious copy number alterations, implying that cell identity recognition can correctly distinguish tumor cells (Fig. 2D). We found the presence of endothelial cells (ECs), fibroblasts, granulosa cells, mononuclear phagocytes (MPs), mural cells, T cells, theca cells in normal ovarian tissue. The primary lesion sample (SCC-09_T) was mainly composed of tumor cells, MPs, and T cells. In the recurrent lesion (SCC-01_T), the main cell type was tumor cells, with only a small number of T cells (Fig. 2E).

Single-cell transcriptomics reveal intra-tumoral heterogeneity in SCCOHT cells

We next explored cancer cells and mutual expression patterns of their marker genes. We detected 19,418 tumor cells from the primary and recurrent tumor sample, which were classified into seven clusters (C1-C7) with different biological functions according to the markers identified for each of these clusters. Primary lesion includes clusters 2 and 6, while recurrent lesion included four clusters (1, 3, 5, 7) (Fig. 3A). Cluster 1 (marked by *HTR2C*, *POU3F3*, and *SOSTDC1*) were characterized as neuronal cell body and had high activity in axon genesis. *HTR2C* encodes a G-protein coupled receptor for 5-hydroxytryptamine, which may modulate the release of Ca^{2+} from intracellular stores [22]. Cluster 2 showed a high level of *NPAS3*, and *ARHGEF28*, both of which play a broad role in neurogenesis. And it is reported that mRNA levels of *ARHGEF28* are associated

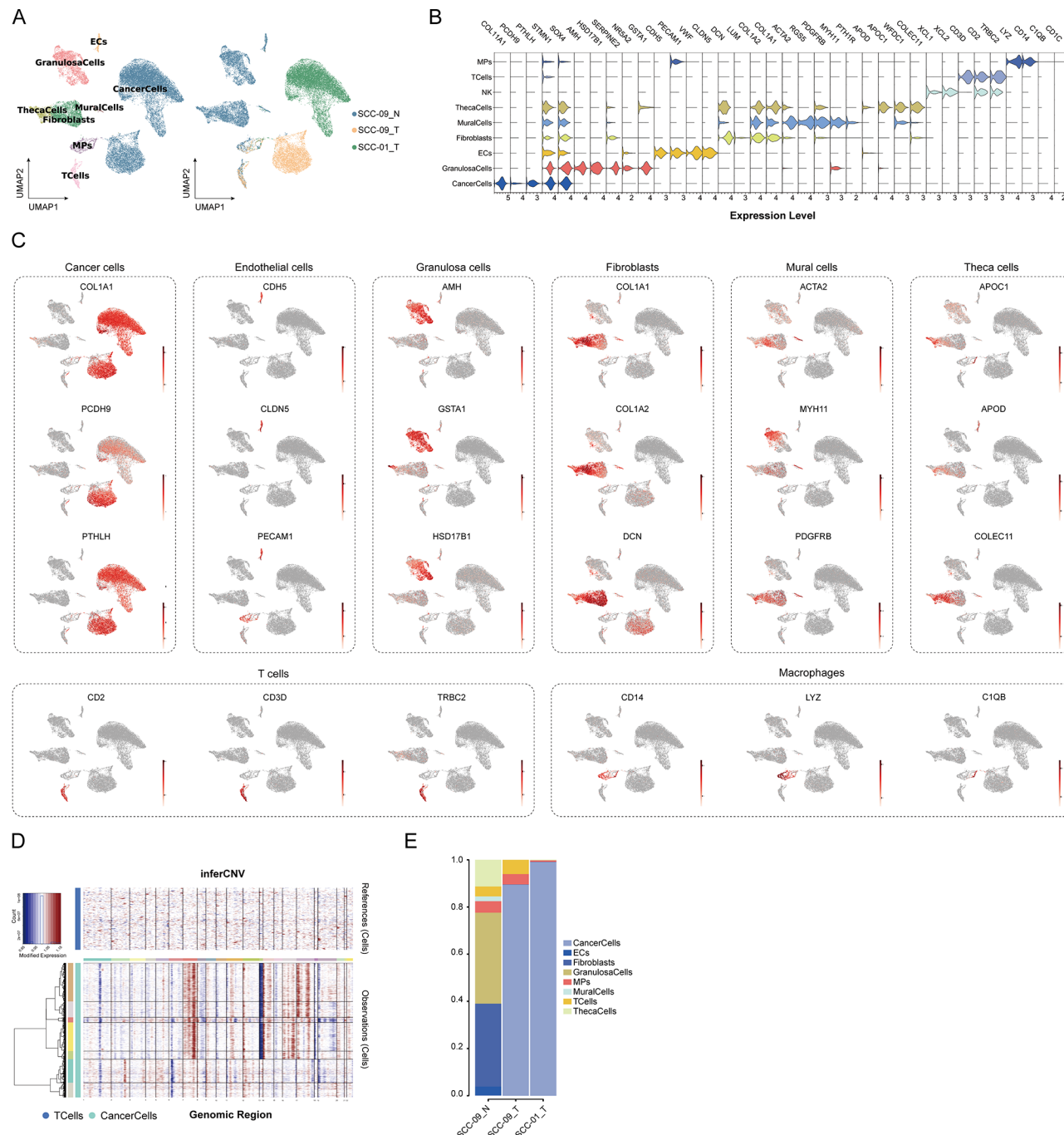


Fig. 2 Single-cell RNA analyses of SCCOHT. **A**, UMAP representation of 8 clusters generated from all tumor cells. The left panel represents the classification of cell types, while the right panel illustrates the specific samples from which these cells originate. **B**, Violin plots presenting the expression level for the selected markers in different clusters. **C**, Expression levels of representative well-known markers across the cell types in SCCOHT. Color key from gray to red indicates relative expression levels from low to high. **D**, Heatmap of the copy number variations in the cancer cells analyzed by the InferCNV pipeline. **E**, Ratio of cellular composition in the specific patient sample

with decreased progression-free and overall survival in patients with ovarian cancer [23]. Cluster 3 (marked by *EMX2*, *NPY*, *RORB*) was described as vesicle lumen and was associated with neutrophil function. The essence of cluster 4 (marked by *NEFM*, *PAM*, *RP11-268G12*) was like cluster 3 but was more inclined towards respiratory

metabolism in biological process. Strong expression of genes related to cell division process observed in cluster 5 (marked by *KIF20A*, *PLK1*, *RRM2*) and may explain the rapid growth in SCCOHT. Cluster 6 exhibited high expression level of *ATP5O*, *PRDX2* and *TMSB4X*. *PRDX2* encodes an antioxidant enzyme, and it may contribute to

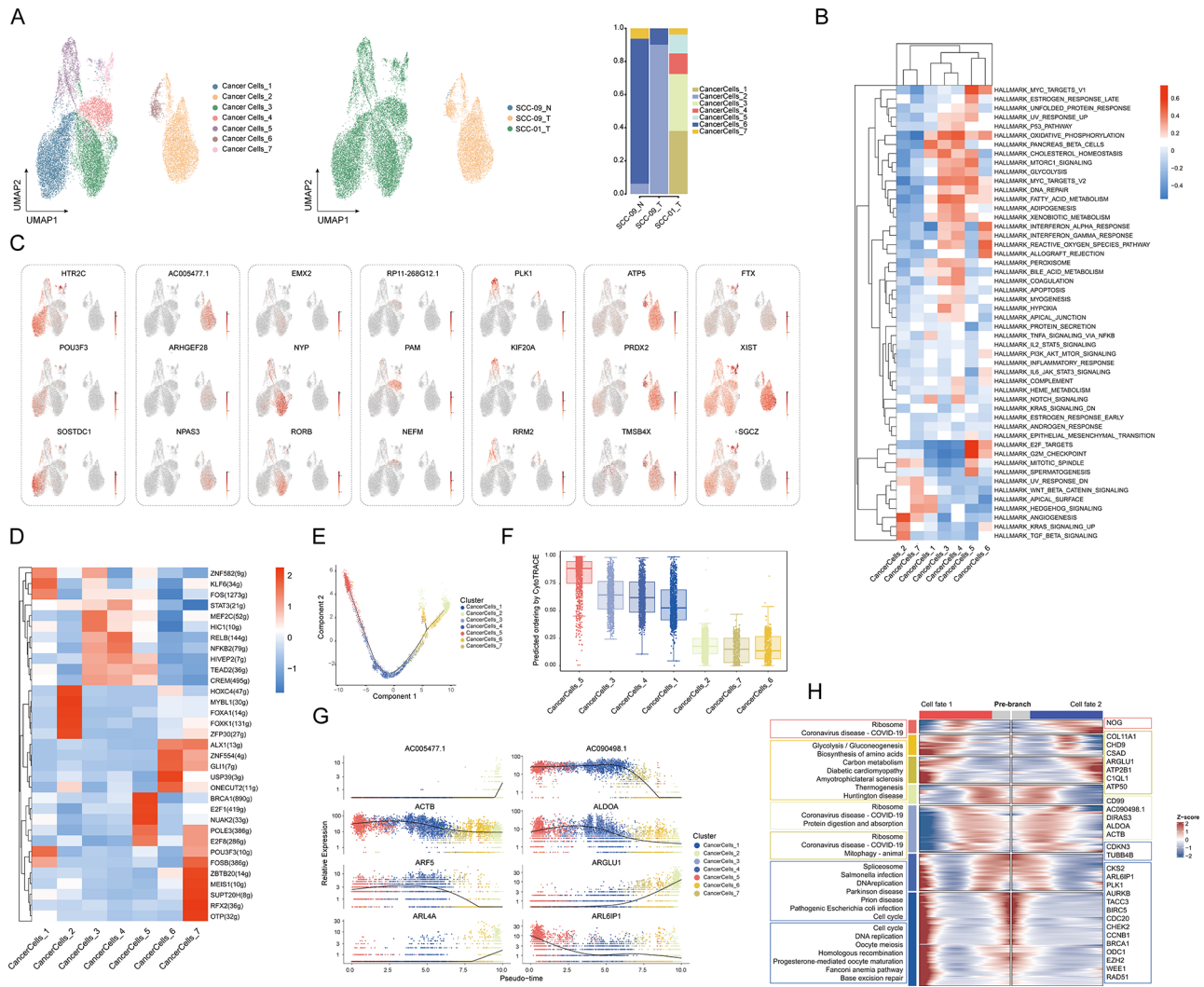


Fig. 3 Heterogeneity of tumor cells in SCCOHT and expression patterns in tumor progression. **A**, The UMAP plot demonstrates the subclusters of cancer cells in primary and recurrent tumor specimens, and the proportion of cell components in specific patient samples is displayed next to it. **B**, Expression levels of representative well-known markers across the different clusters in cancer cells. Color key from gray to red indicates relative expression levels from low to high. **C**, Heatmap showing the enriched hallmark gene signatures of heterogeneity of cells within tumors. **D**, The evolutionary trajectories of these cancer cells. **E**, Box plot comparing the stemness scores in the different clusters. **F**, Expression changes of characteristic genes along the pseudotime. **G**, Heatmap showing the dynamic changes in gene expression along the pseudotime and differential genes and pathways are labeled.

the antiviral activity of CD8⁺ T cells [24]. Cluster 6 was enriched in immune response-related signaling pathways, such as response to interferon-alpha and negative regulation of viral life cycle. Cluster 7 (marked by *FTX*, *SGCZ* and *XIST*) showed higher activity in GABAergic synapse and is enriched in the process of gap junction and calcium signaling pathway (Fig. 3B).

We also conducted GSVA analysis to further explore the heterogeneity of cells within tumors. In primary lesion, angiogenesis, KRAS signaling and TGF- β signaling were enriched in cluster 2; cluster 6 exhibited high activity in interferon response, reactive oxygen species pathway and allograft rejection consistent with GO analysis. In recurrent lesion, pathways related to growth

and development such as Wnt- β catenin signaling and hedgehog signaling were enriched in cluster 7. Clusters 3, 4, and 5 have high level expression of genes related to metabolic pathways (e.g., oxidative phosphorylation, cholesterol homeostasis, glycolysis), DNA repair pathways (e.g., UV response up, DNA repair and p53 pathway). At the same time, cluster 5 was also enriched in cell cycle pathways: E2F targets and G2M checkpoint, supporting the results of GO analysis (Fig. 3C).

Reconstruction of progressive trajectory of cancer cells

We would like to know if there is an evolutionary relationship between these different tumor cells and the factors that contribute to their changes. Pseudo time series

analysis was conducted firstly to explore the evolutionary trajectories of these cancer cells. We found cluster 5 had the highest stemness and gradually differentiated into clusters 2 and 6 (Fig. 3D). CytoTRACE analysis was then applied to predict the differentiation states of these cancer cells and confirmed that cluster 5 has the strongest stemness (Fig. 3E). As the pseudo timing progresses, the expression of *AC005477.1*, *ARGLU1* and *ARL4A* gradually increased, while *ACTB*, *ARF5*, *ARL6IP1* and *ALDOA* gradually decreased (Fig. 3F). We enriched the genes based on the characteristics of expression changes during the pseudo timing process, resulting in a total of seven clusters (C1-C7). Along the trajectory, the gene signature of cluster 1,2,3,4 and 7 were all related to cell division, such as nuclear division, DNA replication, cytoplasmic translation, while cluster 5 was enriched in ATP metabolic process. We also observed that some genes related to cell mitosis (*AURKB*, *CKS2*, *TACC3*, *CHEK2*, *CCNB1*, *CENPE*, *WEE1*), DNA repair (*BRCA1*, *RAD51*) and epigenetic (*EZH2*, *DNMT1*) maintain a high expression in cancer cells of primitive state, although their levels can be high or low in relatively differentiated cells (Fig. 3G).

The characteristics of macrophages in SCCOHT

There were 711 mononuclear phagocytes including macrophages, classical monocytes, non-classical monocyte, and dendritic cells identified in all three samples (Fig. 4A). The most common cell type in normal ovarian tissue is classical monocytes, while the proportion of macrophages in the primary lesion is increased. Macrophages are the main component of mononuclear phagocytes in recurrent lesion (Fig. 4B and Supplementary Table S3).

Tumor-associated macrophages (TAM) are an important component of the immune microenvironment, playing a role in angiogenesis, extracellular matrix remodeling, cancer cell proliferation, metastasis, and immune suppression, as well as resistance to chemotherapy drugs and checkpoint blockade immunotherapy [25]. Recently, a unified nomenclature for TAM subsets was coined on the basis of the signature genes, enriched pathways and predicted function including seven TAM subsets as interferon-primed TAMs (IFN-TAMs), immune regulatory TAMs (reg-TAMs), inflammatory cytokine-enriched TAMs (inflam-TAMs), lipid-associated TAMs (LA-TAMs), pro-angiogenic TAMs (angio-TAMs), resident-tissue macrophage-like TAMs (RTM-TAMs) and proliferating TAMs (prolif-TAMs) [26].

We compared the differential genes of macrophages in primary and recurrent lesions with those in normal ovarian tissue and found that macrophages in primary lesion exhibited high expression level of *APOE*, *APOC1*, *SPP1*, which are markers of LA-TAMs (Fig. 4C). Consistent with this, GO analysis showed an enhanced functions

of regulation of lipid transport, regulation of lipid localization, endocytic vesicle in primary tumor (Fig. 4D). It has been reported that enhanced lipid accumulation and metabolism are required for the differentiation and activation of TAMs suppressing anti-tumor immune responses and perhaps promote tumor progression [27, 28]. Different from primary lesion, high expressions of *CCL3L3* and *CCL4L2* in macrophages in recurrent lesion were observed suggesting inflam-TAMs (Fig. 4E). Inflam-TAMs have an expression signature of inflammatory cytokines and might actively recruit and regulate immune cells during the tumor-associated inflammatory response. GO analysis further confirmed the upregulation in neutrophil degranulation, neutrophil activation, and chemokine activity (Fig. 4F). We also found macrophages in recurrent lesion expressed high level of *HLA-DRB5* representing Reg-TAMs.

The characteristics of T cells in SCCOHT

The number of T cells in the primary lesion is like normal ovarian tissue, but the proportion of T cells in the primary lesion is higher than that in normal ovarian tissue (6.7% vs. 4.2%), while the number of T cells in the recurrent lesion is only 10 with a proportion of 0.07% (Supplementary Table S3). We further classified T cells into eight subtypes, totaling 700 cells, including *KLRF1*⁺ NK cells, *XCL1*⁺ NK cells, *TRGC1*⁺ NKT cells, *FCGR3A*⁺ NKT cells, exhausted *PDCD1*⁺*CD8*⁺ T cells, effector *CD27*⁺*CD8*⁺ T cells, effector *CCR5*⁺*CD8*⁺ T cells and *CCR7*⁺ Naïve T cells (Fig. 5A and B). Compared to normal ovarian tissue, the proportion of exhausted *CD8*⁺ T cells was higher in tumor especially in recurrent lesion (Fig. 5C). Then we conducted GSVA analysis on these T cell subsets and found that compared to normal ovaries, *CCR5*⁺*CD8*⁺ T cells and *CCR7*⁺ Naïve T cells in the primary lesion had higher gene expression of exhaustion, while exhausted *PDCD1*⁺*CD8*⁺ T cells had higher gene expression of ferroptosis (Fig. 5D).

To further confirm the results obtained from scRNA-seq, we also performed mIF staining on normal ovarian tissue, three primary lesions, and three recurrent lesions. The number of T cells infiltrating the SCCOHT tumor was higher than those in normal ovarian tissue. And there was no significant difference in the number of *CD4*⁺ and *CD8*⁺ T cells between the recurrent and primary lesions, but the number and ratio of *PDI*⁺*CD4*⁺ T cells and *PDI*⁺*CD8*⁺ T cells were higher in recurrent lesion, and SCC-08 exhibited the highest level of PD-1 (Fig. 5E and F). To summarize, we observed infiltration of exhausted T cells in SCCOHT tumors, but there was heterogeneity between patients.

In addition, we tended to figure out the interaction between immune cells in the primary lesion and normal ovarian tissue and cell-cell interaction analysis was

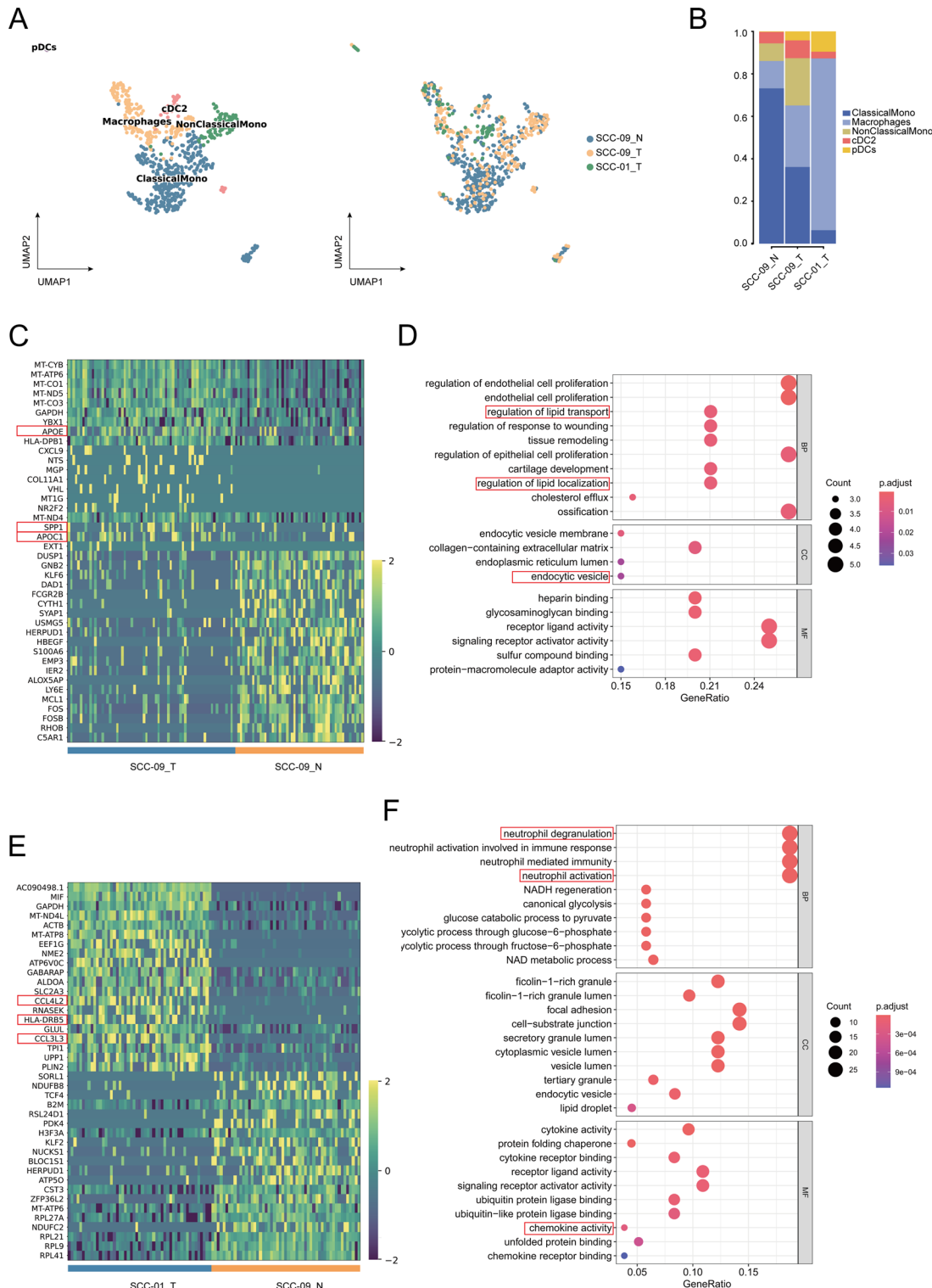


Fig. 4 The characteristics of macrophages in SCCOHT. **A**, The UMAP diagram shows different components of mononuclear phagocytes identified in three samples. **B**, The proportion of each cell type in three samples. **C**, Heatmap of differential expression genes between primary lesion and normal ovarian tissue. **D**, Upregulated signaling pathways of macrophages in the primary lesion compared to those in normal ovarian tissue analyzed by GO. **E**, Heatmap of differential expression genes between recurrent lesion and normal ovarian tissue. **F**, Upregulated signaling pathways of macrophages in the recurrent lesion compared to those in normal ovarian tissue analyzed by GO

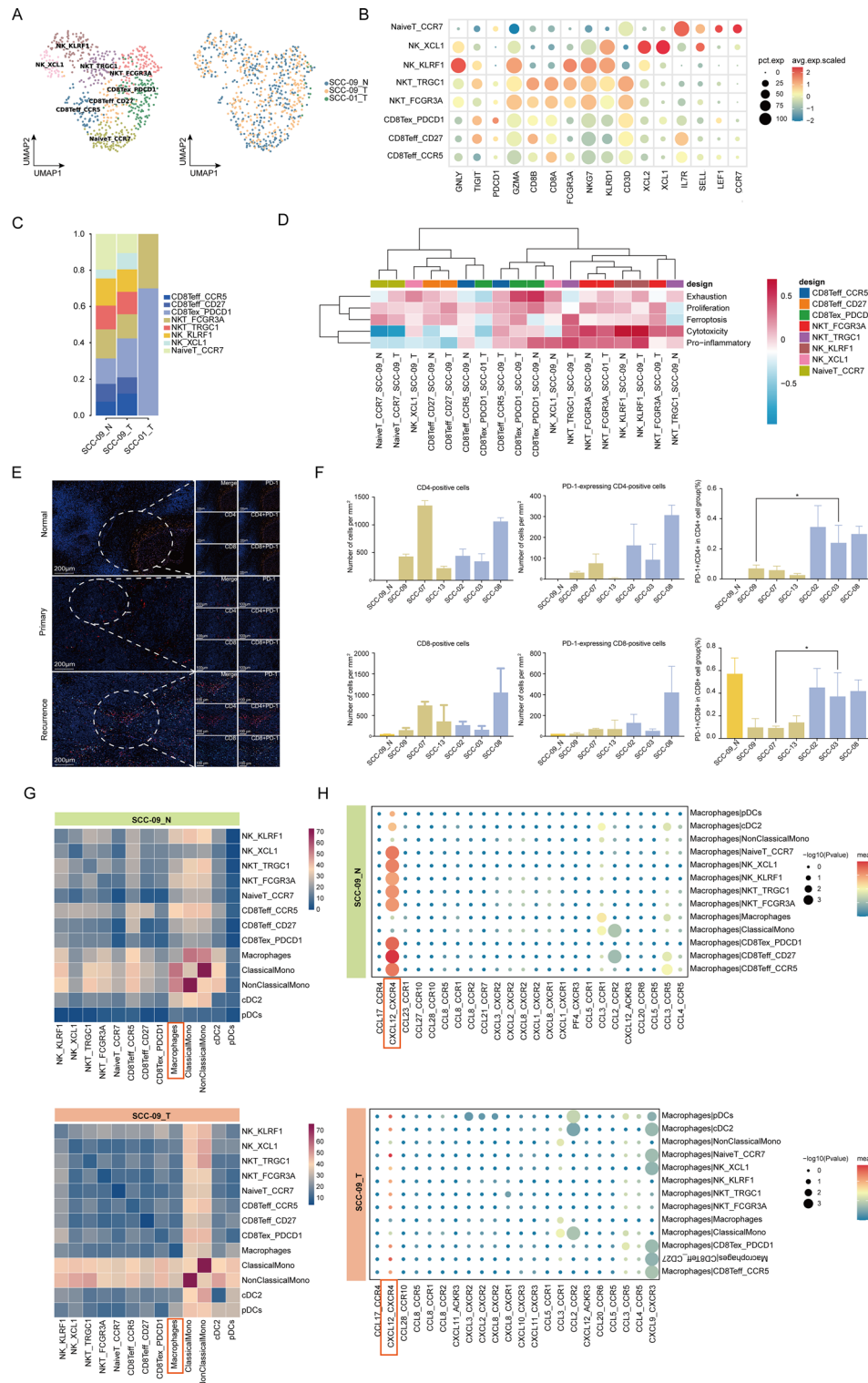


Fig. 5 (See legend on next page.)

conducted. The results showed that compared with normal ovarian tissue, the interaction between macrophages and T cells in the primary lesion was weakened (Fig. 5G). Furthermore, we found that the interaction between

CXCL12 ligands secreted by macrophages and CXCR4 receptors of T cell was significantly reduced (Fig. 5H).

(See figure on previous page.)

Fig. 5 The characteristics of T cells in SCCOHT. **A**, The UMAP diagram shows different components of T cells identified in three samples. **B**, Dot plots indicating the differentially expressed genes in eight T cell subtypes. **C**, The portion of T cell subtypes in the three samples. **D**, the heatmap displays the gene expression characteristics of various T cell subpopulations analyzed by GSVA. **E**, Representative images of mIF staining with the PD-1, CD4, and CD8 antibodies of normal ovarian tissue, primary lesion, and recurrent lesion (Scale bars, 200 μ m). Enlarged inset shows the infiltration of T cells expressing various marker genes and cells co-expressing PD-1 and CD4/CD8 (Scale bars, 100 μ m). **F**, CD4-positive, CD8-positive, PD-1-expressing CD4-positive and PD-1-expressing CD8-positive cell counts per mm². The y-axis indicates number of marker-positive cells, and the x-axis indicates SCCOHT cases. Percentage of PD-1-positive cells out of all CD4/CD8 cells. The y-axis indicates percentage of PD-L1-expressing T cells, and the x-axis indicates SCCOHT cases (* $P<0.05$). **G**, the heatmap displays the interaction between two cell types, with darker colors indicating a greater number of interactions between the two cell types. **H**, the bubble plot illustrated the predicted chemokine interactions between macrophages as ligand cells and other cell types

Discussion

Our results showed that 86.7% (13 in 15) patients exhibited inactivation mutations of *SMARCA4*. The scRNA-seq results of the two SCCOHT cases we reported suggest the presence of intra-tumoral heterogeneity and immune microenvironment.

The LOH of *SMARCA4* in SCCOHT is universal, both in our cohort and literatures. It was revealed that *SMARCA4* was the only gene with recurrent mutations in SCCOHT, with a frequency of over 80% and the frequency of LOH reached 40.6% (13/32) and 66.7% (8/12) [3, 4, 29]. Our results showed LOH occurred in 10/15 (66.7%) cases. *SMARCA4* mutations occurred throughout various exons and included nonsense, frameshift, and splice-site mutations as well as a homozygous intragenic deletion of two exons. We did not observe hot spot mutations of *SMARCA4* in our cohort and the loss of function of the coding protein seemed to be the cause of the disease.

SCCOHT tumors progress rapidly and are highly prone to drug resistance and recurrence, suggesting the complex components in this type of neoplasm. We depicted the cellular heterogeneity within the primary and recurrent lesions in-depth through scRNA-seq and the recurrent lesion exhibited highest stemness. Genes related to cell mitosis were upregulated in these "stem-like" cells, such as *AURKB*, *CCNB1*, *WEE1*, *CHEK2* and so on. In the future, we can focus on these targets in the treatment of SCCOHT.

Through scRNA-seq, two main types of immune cells were observed in the two cases of SCCOHT tumor microenvironment, namely macrophages, and T cells. A previous study observed biologically significant levels of $CD3^+$ T cell infiltration in recurrent lesion after chemotherapy and macrophages was the most abundant PD-L1-positive cells in some tumor [9]. Our study additional added normal ovarian tissue and primary lesions to observe the infiltration of different type of T cells in SCCOHT. mIF staining results showed infiltration of $CD4^+$ / $CD8^+$ T cells in tumor tissues, and the $CD4^+$ / $CD8^+$ T cells in the recurrent lesion showed high levels of PD-1 expression, basically consistent with the results reported in the above literature. It was worth noting that although the proportion of exhausted T cell in the recurrent lesion was high according to scRNA-seq results,

the total number of T cells was small, which may be related to individual differences. In the primary lesion we reported here, macrophages were mainly LA-TAMs while in the recurrent lesion, those were inflam-TAMs. TAM targeting has received significant attention, but the vast majority are still in clinical trials [26]. Its application in the clinical treatment of SCCOHT still needs to be explored. It has been reported that CXCL12 and its receptor may contribute to TAMs-mediated $CD8^+$ T cell suppression [30], but the influence of weakened interaction in SCCOHT remains to be explored.

Our research also has several limitations. Firstly, our sample size is relatively small, comprising only one case each of normal ovarian tissue, primary lesion, and recurrent lesion, which may not be representative of the majority of patients. Secondly, the recurrent lesion and primary lesion are not from the same patient, which means that the comparison between them may primarily reflect inter-individual differences rather than the true distinctions between primary and metastatic disease. It is important to emphasize that our findings are based on individual case reports and require further validation in future studies. The patient with the primary lesion reported in this article has remained stable so far, and if the disease progresses in the future, we may obtain recurrent lesions from the same patient for more accurate comparative analysis.

In conclusion, we examined SCCOHT using WES and single-cell RNA sequencing, revealing intra-tumoral heterogeneity and the immune microenvironment in a Chinese cohort. This is the first study to characterize SCCOHT at single-cell resolution, identifying potential therapeutic targets such as CHEK2, CCNB1, WEE1, as well as distinct TAM subsets. These findings provide new insights into SCCOHT pathogenesis and highlight promising strategies for targeted therapy and immunotherapy to improve clinical outcomes.

Supplementary Information

The online version contains supplementary material available at <https://doi.org/10.1186/s13048-025-01649-8>.

Supplementary Material 1

Supplementary Material 2

Supplementary Material 3

Author contributions

Y. Gao: Data curation, formal analysis, validation, writing—original draft, writing—review and editing. K.-W. Zheng: Data curation, formal analysis. M.-Y. Kang: Data curation, investigation, writing—review and editing. H.-W. Tan: Validation, writing—original draft. B.-J. Lu: Conceptualization, resources, data curation. L. Chen: Conceptualization, resources, data curation. J. Xu: Data curation, validation, investigation, writing—review and editing. C. Lu: Software, formal analysis, visualization, methodology. R.-R. Chai: Software, formal analysis, visualization, methodology. C.-J. Xu: Conceptualization, resources, supervision, project administration. Y. Kang: Supervision, investigation, project administration, writing—review and editing.

Funding

National Key Research and Development Program of China (2022YFC2705004) and Shanghai Clinical Research Center for Gynecological Diseases (22MC1940200).

Data availability

Data can be obtained by contacting the corresponding author.

Declarations**Human ethics and consent to participate declarations**

The study was conducted according to the guidelines of the Declaration of Helsinki, and approved by the Ethics Committee of the Obstetrics and Gynecology Hospital of Fudan University (IRB: 2018-31). Informed consent for the use of clinical samples for medical study and the publication of results was provided by the patient.

Competing interests

The authors declare no competing interests.

Author details

¹Department of Obstetrics and Gynecology, Obstetrics and Gynecology Hospital, Fudan University, Shanghai 200011, China

²Department of Obstetrics and Gynecology of Shanghai Medical School, Fudan University, Shanghai 200032, China

³Shanghai Key Laboratory of Female Reproductive Endocrine Related Diseases, Shanghai 200011, China

⁴Department of Surgical Pathology, School of Medicine, Women's Hospital, Zhejiang University, Hangzhou, Zhejiang 310006, China

⁵SynerGene, Ganzhou, Jiangxi 342604, China

⁶Department of Pathology, Tianjin Central Hospital of Gynecology & Obstetrics, Tianjin 300052, China

Received: 15 April 2024 / Accepted: 15 March 2025

Published online: 09 April 2025

References

- Young RH, Oliva E, Scully RE. Small cell carcinoma of the ovary, hypercalcemic type. A clinicopathological analysis of 150 cases. Am J Surg Pathol. 1994;18(11):1102–16.
- Errico A, Genetics. SMARCA4 mutated in SCCOHT. Nat Rev Clin Oncol. 2014;11(6):302.
- Jelinic P, Mueller JJ, Olvera N, Dao F, Scott SN, Shah R, et al. Recurrent SMARCA4 mutations in small cell carcinoma of the ovary. Nat Genet. 2014;46(5):424–6.
- Ramos P, Karnezis AN, Craig DW, Sekulic A, Russell ML, Hendricks WP, et al. Small cell carcinoma of the ovary, hypercalcemic type, displays frequent inactivating germline and somatic mutations in SMARCA4. Nat Genet. 2014;46(5):427–9.
- Auguste A, Blanc-Durand F, Deloger M, Le Formal A, Bareja R, Wilkes DC et al. Small cell carcinoma of the ovary, hypercalcemic type (SCCOHT) beyond SMARCA4 mutations: A comprehensive genomic analysis. Cells. 2020;9(6).
- Wang Y, Chen SY, Karnezis AN, Colborne S, Santos ND, Lang JD, et al. The histone methyltransferase EZH2 is a therapeutic target in small cell carcinoma of the ovary, hypercalcemic type. J Pathol. 2017;242(3):371–83.
- Lang JD, Hendricks WPD, Orlando KA, Yin H, Kiefer J, Ramos P, et al. Ponatinib shows potent antitumor activity in small cell carcinoma of the ovary hypercalcemic type (SCCOHT) through multikinase inhibition. Clin Cancer Res. 2018;24(8):1932–43.
- Xue Y, Meehan B, Macdonald E, Venneti S, Wang XQD, Witkowski L, et al. CDK4/6 inhibitors target SMARCA4-determined Cyclin D1 deficiency in hypercalcemic small cell carcinoma of the ovary. Nat Commun. 2019;10(1):558.
- Jelinic P, Ricca J, Van Oudenhoove E, Olvera N, Merghoub T, Levine DA, et al. Immune-Active microenvironment in small cell carcinoma of the ovary, hypercalcemic type: rationale for immune checkpoint Blockade. J Natl Cancer Inst. 2018;110(7):787–90.
- Dura B, Choi JY, Zhang K, Damsky W, Thakral D, Bosenberg M, et al. scFTD-seq: freeze-thaw Lysis based, portable approach toward highly distributed single-cell 3' mRNA profiling. Nucleic Acids Res. 2019;47(3):e16.
- Cortat A, Martignetti L, Six E, Rausell A. Gene signature extraction and cell identity recognition at the single-cell level with Cell-ID. Nat Biotechnol. 2021;39(9):1095–102.
- Butler A, Hoffman P, Smibert P, Papalexi E, Satija R. Integrating single-cell transcriptomic data across different conditions, technologies, and species. Nat Biotechnol. 2018;36(5):411–20.
- Yu G, Wang LG, Han Y, He QY. ClusterProfiler: an R package for comparing biological themes among gene clusters. Omics. 2012;16(5):284–7.
- Hänzelmann S, Castelo R, Guinney J. GSVA: gene set variation analysis for microarray and RNA-seq data. BMC Bioinformatics. 2013;14:7.
- Gulati GS, Sikandar SS, Wesche DJ, Manjunath A, Bharadwaj A, Berger MJ, et al. Single-cell transcriptional diversity is a hallmark of developmental potential. Science. 2020;367(6476):405–11.
- Qiu X, Hill A, Packer J, Lin D, Ma YA, Trapnell C. Single-cell mRNA quantification and differential analysis with census. Nat Methods. 2017;14(3):309–15.
- Tirosh I, Venteicher AS, Hebert C, Escalante LE, Patel AP, Yizhak K, et al. Single-cell RNA-seq supports a developmental hierarchy in human oligodendrogloma. Nature. 2016;539(7628):309–13.
- Efremova M, Vento-Tormo M, Teichmann SA, Vento-Tormo R. CellPhoneDB: inferring cell-cell communication from combined expression of multi-subunit ligand-receptor complexes. Nat Protoc. 2020;15(4):1484–506.
- Lin DI, Chudnovsky D, Duggan B, Zajchowski D, Greenbowe J, Ross JS, et al. Comprehensive genomic profiling reveals inactivating SMARCA4 mutations and low tumor mutational burden in small cell carcinoma of the ovary, hypercalcemic-type. Gynecol Oncol. 2017;147(3):626–33.
- Witkowski L, Goudie C, Ramos P, Boshari T, Brunet JS, Karnezis AN, et al. The influence of clinical and genetic factors on patient outcome in small cell carcinoma of the ovary, hypercalcemic type. Gynecol Oncol. 2016;141(3):454–60.
- Mandelker D, Ceyhan-Birsoy O. Evolving significance of Tumor-Normal sequencing in cancer care. Trends Cancer. 2020;6(1):31–9.
- Lu K, Hong Y, Tao M, Shen L, Zheng Z, Fang K, et al. Depressive patient-derived GABA interneurons reveal abnormal neural activity associated with HTR2C. EMBO Mol Med. 2023;15(1):e16364.
- Kleinschmidt EG, Miller NLG, Ozmadenci D, Tancioni I, Osterman CD, Barrie AM, et al. Rgnf promotes ovarian tumor progression and confers protection from oxidative stress. Oncogene. 2019;38(36):6323–37.
- Liang H, Zhang S, Ma Y, Wang H, Cao Z, Shi R, et al. Elucidating the cell metabolic heterogeneity during hematopoietic lineage differentiation based on Met-Flow. Int Immunopharmacol. 2023;121:110443.
- Mantovani A, Allavena P, Marchesi F, Garlanda C. Macrophages as tools and targets in cancer therapy. Nat Rev Drug Discov. 2022;21(11):799–820.
- Cassetta L, Pollard JW. A timeline of tumour-associated macrophage biology. Nat Rev Cancer. 2023;23(4):238–57.
- Su P, Wang Q, Bi E, Ma X, Liu L, Yang M, et al. Enhanced lipid accumulation and metabolism are required for the differentiation and activation of Tumor-Associated macrophages. Cancer Res. 2020;80(7):1438–50.
- Di Conza G, Tsai CH, Gallart-Ayala H, Yu YR, Franco F, Zaffalon L, et al. Tumor-induced reshuffling of lipid composition on the Endoplasmic reticulum membrane sustains macrophage survival and pro-tumorigenic activity. Nat Immunol. 2021;22(11):1403–15.
- Witkowski L, Carrot-Zhang J, Albrecht S, Fahiminiya S, Hamel N, Tomiak E, et al. Germline and somatic SMARCA4 mutations characterize small cell carcinoma of the ovary, hypercalcemic type. Nat Genet. 2014;46(5):438–43.
- Qin R, Ren W, Ya G, Wang B, He J, Ren S, et al. Role of chemokines in the crosstalk between tumor and tumor-associated macrophages. Clin Exp Med. 2023;23(5):1359–73.

Publisher's note

Springer Nature remains neutral with regard to jurisdictional claims in published maps and institutional affiliations.